Fast Track Communications

IOP Publishing | Institute of Physics and Engineering in Medicine Physics in Medicine & Biology

Phys. Med. Biol. **61** (2016) L20–L28 doi:10.1088/0031-9155/61/12/L20

Fast Track Communication

Scattering and reflection identification in H-scan images

K J Parker

Department of Electrical and Computer Engineering, University of Rochester, Hopeman Building 203, PO Box 270126, Rochester, NY 14627-0126, USA

E-mail: kevin.parker@rochester.edu

Received 12 January 2016, revised 21 April 2016
Accepted for publication 28 April 2016
Published 25 May 2016

Abstract

Medical ultrasound imaging scanners typically display the envelope of the reflected signal on a log scale. The properties of this image and speckle patterns from collections of scatterers have a number of well-known disadvantages. One is the inability to differentiate between different scatterers that may have fundamentally different frequency-dependent scattering cross sections. This study proposes a framework for characterizing scattering behavior and visualizing the results as color coding of the B-scan image. The methodology matches a model of pulse-echo formation from typical situations to the mathematics of Gaussian weighted Hermite functions. The results show an ability to reveal some of the information otherwise hidden in the conventional envelope display, and can be generalized to more conventional bandlimited pulse functions. This new class of images is termed H-scan where 'H' stands for 'Hermite' or 'hue' to distinguish it from conventional B-scan format.

Keywords: ultrasound, imaging, tissue characterization, scattering, Hermite functions

(Some figures may appear in colour only in the online journal)

1. Introduction

B-Scan images are based on specular reflections and scattering from changes in acoustic impedance within different tissues (Prince and Links 2006, Cobbold 2007). A long-standing question in biomedical ultrasound concerns the frequency dependence of scatterers within different tissues, organs, and the blood. These tissue characterization techniques for scattering include measurements of the frequency dependence and angular dependence of backscattered waves. An excellent overview of these approaches to characterize scattering is found in chapter 9 of Szabo (2004). Many of the statistical techniques require a sufficient ensemble

 © 2016 Institute of Physics and Engineering in Medicine Printed in the UK

average over which to calculate the expected value of measured quantity. Given the statistics of speckle (Burckhardt 1978, Lizzi *et al* 1997a), this can limit the resolution or accuracy of statistical approaches. Accordingly, we seek an alternative where the received echoes can be identified or associated with major classes of signals from tissues. These are linked to the mathematics of Gaussian weighted Hermite polynomials so that the overall identification task can be simplified.

2. Theory

Under a number of reasonable assumptions, it is possible to model the pulse-echo A-line formation as a convolution of an incident pulse with a sequence of reflections (Macovski 1983, Cobbold 2007). Assuming sufficiently weak attenuation, backscatter, and focusing, the integration can be reduced to a convolution model (Macovski 1983) such that the received echo $e(t)$ is approximated by

$$e(t) = A\left\{ p(t)s(x,y) \ast\ast\ast R\left(x, y, \frac{ct}{2}\right)\right\} \tag{1}$$

where A is an amplitude constant, $p(t)$ is the propagating pulse in the axial direction, $s(x,y)$ is the beam width in the transverse and elevational axes (and thus the beam pattern is assumed to be a separable function, and $R(x,y,z)$ is the 3D pattern of reflectors or scatterers. The speed of the sound is c, and with a round trip for the echo the axial distance z is replaced by $ct/2$ in the 3D convolution represented by the symbol $\ast\ast\ast$.

In simplified 1D derivations with an assumption of small spatial variations in the acoustic impedance $Z = \rho c$, the function R can be shown to be related to the spatial derivative of Z in the direction z of propagation of the imaging pulse (Macovski 1983):

$$R(z) \approx \left(\frac{1}{2Z_0}\right)\frac{\mathrm{d}Z(z)}{\mathrm{d}z}. \tag{2}$$

This relationship implies that specific structures yield characteristic reflections. A small incremental step function in acoustic impedance, along the direction of the propagating pulse, yields an impulse function for $R(z)$. The returning echo is then simply $R \cdot p(t)$. However, a thin layer of material with increased impedance yields a positive impulse at the front surface and a negative impulse at the back surface. In the limit this approaches the doublet function, $\delta'(t)$, the derivative of the Dirac delta function. In this case, the returned echo is proportional to the derivative of $p(t)$ with respect to time. This implies a frequency content weighted by ω since a property of Fourier Transforms is (Bracewell 1986)

$$\Im\left\{\frac{\mathrm{d}p(t)}{\mathrm{d}t}\right\} \rightarrow j\omega P(\omega), \tag{3}$$

where $\Im\{\}$ is the Fourier transform operation and $P(\omega)$ is the Fourier transform of $p(t)$.

Finally, in more general scattering theory, the Born approximation for a small (subwavelength) spherical scatterer has a leading term for scattered pressure that is proportional to ω^2 (Morse and Ingard 1987). Furthermore, a cloud of small, weak scatterers, incoherently spaced, similarly has a scattered pressure dependence with a leading term proportional to ω^2 (Morse and Ingard 1987). Larger scatterers and random collections of scatterers with spatial correlation functions will have more complicated scattering versus frequency formulas (Waag *et al* 1982, Campbell and Waag 1983, 1984, Waag 1984, Lerner and Waag 1988, Mottley and Miller 1988, 1990).

Table 1. Gaussian weighted Hermite polynomials.

Order, n		Energy
n	$\mathrm{H}_n\mathbf{G}$	E
0	$(1)\mathbf{G}$	$\sqrt{\pi/2}$
1	$(2t)\mathbf{G}$	$\sqrt{\pi/2}$
2	$(4t^2-2)\mathbf{G}$	$3\sqrt{\pi/2}$
3	$(8t^3-12t)\mathbf{G}$	$15\sqrt{\pi/2}$
4	$(16t^4-48t^2+12)\mathbf{G}$	$105\sqrt{\pi/2}$
5	$(32t^5-160t^3+120t)\mathbf{G}$	$945\sqrt{\pi/2}$

Notation: $\mathbf{G}=\mathbf{e}(-t^2)$. Energy $=\int_{-\infty}^{\infty}\mathbf{G}^2H_n^2\mathrm{d}t = 1\times3\times5\times\ldots\times|2n-1|\times\sqrt{\pi/2}$.

However, the ω^2 frequency weighting is an important analytical endpoint because by Fourier transform theorems, an ω^2 weighting corresponds to the second derivative of a function:

$$\Im\left\{\frac{\mathrm{d}^2p(t)}{\mathrm{d}t^2}\right\}\rightarrow\omega^2P(\omega) \tag{4}$$

To recap, within some degree of approximation, the echo or reflection from an incremental step function of impedance produces an echo proportional to $p(t)$. A thin layer of incrementally higher impedance produces an echo proportional to $\mathrm{d}p/\mathrm{d}t$. A cloud of small weak scatterers produces an echo proportional to $\mathrm{d}^2p/\mathrm{d}t^2$. Given this, we seek to identify echoes by their relationship to the transmitted pulse and its derivatives. A family of functions related to the Hermite polynomials is one convenient way to do this.

2.1. Gaussian weighted Hermite polynomials

The successive differentiation of the Gaussian pulse $\mathbf{e}(-t^2)$ generates the nth order Hermite polynomial (see table 1) (Poularikas 2010). The Hermite polynomials are defined by the formula

$$\begin{aligned} H_n(t) &= (-1)^n\mathbf{e}^{t^2}\frac{\mathrm{d}^n}{\mathrm{d}t^n}\mathbf{e}^{-t^2} \\ n &= 0,1,2\ldots;t\in\pm\infty \end{aligned} \tag{5}$$

When multiplied by an envelope $\mathbf{G}=\mathbf{e}^{-t^2}$, these become the Gaussian weighted Hermite polynomials.

Note that these Gaussian weighted Hermite polynomials do not possess orthogonality properties unlike the longer duration Hermite functions (Abramowitz and Stegun 1964, Poularikas 2010). They do have a useful relation with respect to time derivative: $\frac{\mathrm{d}}{\mathrm{d}t}(\mathbf{G}\cdot H_n(t)) = -\mathbf{G}\cdot H_{n+1}(t)$.

Also, the $GH_4(t)$ function resembles a typical broadband pulse. If a transducer element has a one-way transfer function of

$$h(t)=\mathbf{e}^{-t^2/(1/2)}\left[1+H_2(t)\right]=\mathbf{e}^{-t^2/(1/2)}\left[4t^2-1\right], \tag{6}$$

then it can be easily shown that the two-way (transmit-receive) impulse response is:

$$h(t)*h(t)=\left(\frac{\sqrt{2}}{64}\right)\mathbf{e}^{-t^2/1}H_4(t)=A_0\mathbf{G}H_4(t). \tag{7}$$

Table 2. Match of signals and structures assuming a $\mathbf{G}H_4(t)$ transmit.

Tissue structure	Reflection class $R(t)$	Frequency weighting	Hermite function class
Flat interface (specular)	$\delta(t)$ (Dirac delta)	1	$\mathbf{G}H_4(t)$
Thin layer	$\frac{\mathrm{d}\delta(t)}{\mathrm{d}t}$	$j\omega$	$\mathbf{G}H_5(t)$
Small scatterers	$\frac{\mathrm{d}^2\delta(t)}{\mathrm{d}t^2}$	ω^2	$\mathbf{G}H_6(t)$

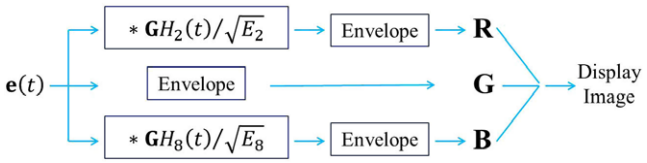

Figure 1. Schematic for parallel processing and display of received echoes $\mathbf{e}(t)$. Convolution with a lower frequency and lower order GWHF is assigned red, and higher frequency/higher order GWHF assigned blue. The envelope is used for green and retains the highest original axial resolution.

Assuming a pulse-echo system has a round trip impulse response of $A_0\mathbf{G}H_4(t)$, then from the logic of equations (2)–(4) we expect that a reflection $R(z)$ from a step function of acoustic impedance will be represented by a delta function $R_0\delta(t)$ and thus a corresponding received echo proportional to $\mathbf{G}H_4(t)$. In other words, equation (2) becomes, in simplest 1D form:

$$\mathbf{e}_1(t) = (A_0\mathbf{G}H_4(t)) * R_0\delta(t) = RA_0\mathbf{G}H_4(t) \tag{8}$$

However, a thin layer of higher impedance would approximate a discrete doublet or derivative $\delta'(t)$ as a reflector and return an echo proportional to $\mathbf{G}H_5(t)$ because of the derivative nature of the Hermite polynomials:

$$\mathbf{e}_2(t) = (A_0\mathbf{G}H_4(t)) * R_2\delta'(t) = -R_2A_0\mathbf{G}H_5(t). \tag{9}$$

Finally, a small scatterer or incoherent cloud of small scatterers would exhibit a second derivative behavior and return an echo proportional to $\mathbf{G}H_6(t)$. The relationships are summarized in table 2.

In this framework, the identification task is simply to classify echoes by similarity to either $\mathbf{G}H_4(t)$, or $\mathbf{G}H_5(t)$, or $\mathbf{G}H_6(t)$. A natural classification test employing the concept of matched filters (Lathi 1983) in parallel or maximum likelihood filters (Proakis 2001) would suggest a convolution of the received signal with scaled versions of $\mathbf{G}H_4(t)$, or $\mathbf{G}H_5(t)$, $\mathbf{G}H_6(t)$ to form three post-processed signals. One could simply select the maximum value at each point in time or display the relative strength as colors.

The disadvantages of this are twofold. First, each convolution results in some loss of resolution, and secondly, the cross-correlation terms between $\mathbf{G}H_4(t)$ and $\mathbf{G}H_5(t)$, and similarly for $\mathbf{G}H_6(t)$ and $\mathbf{G}H_5(t)$ are substantial due to the significant overlap of spectra. Thus, a simpler approach uses the classic envelope as intensity (or 'G' in RGB) with two parallel convolution filters applied to gauge the relative strength of the echoes with respect to $\mathbf{G}H_4(t)$ and $\mathbf{G}H_6(t)$. In practice, discrimination can be improved by using more emphasis on the extremes of the spectra, for example $\mathbf{G}H_2(t)$ and $\mathbf{G}H_8(t)$, each normalized by $\sqrt{E_n}$. A simplified flow chart is shown in figure 1.

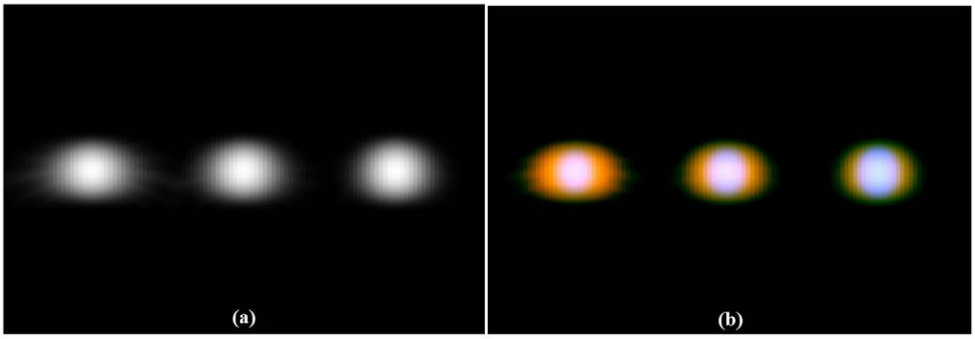

Figure 2. Simulated 5 MHz scan of three scatterers, modeling a discrete singlet, doublet, and triplet. (a) Conventional 50 dB B-scan image of the envelope demonstrates three scatterers with only a subtle difference in transverse width. (b) Color coding from Hermite convolution reveals the intrinsic frequency weighting of the different scatterers.

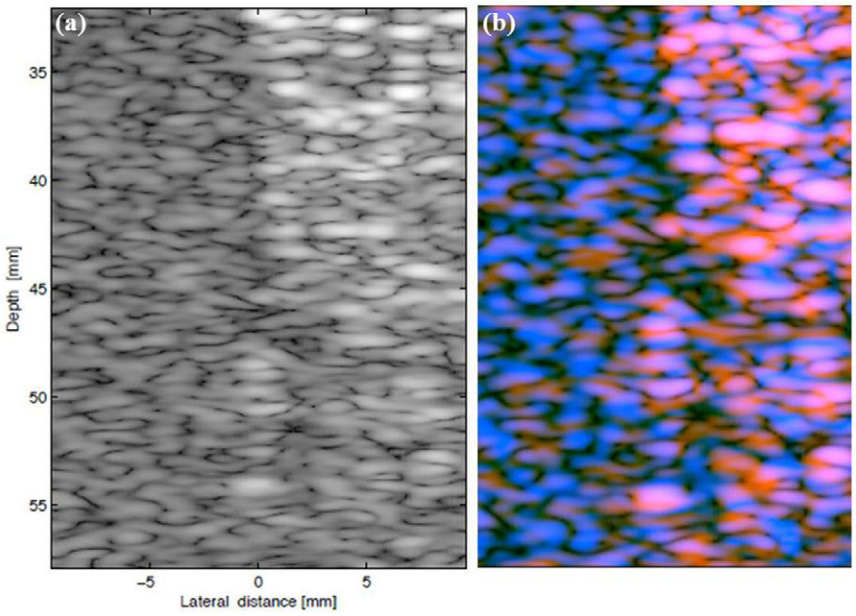

Figure 3. Five MHz scan of small versus large scatterers in a gelatin phantom. (a) Black and white, conventional B-scan. (b) Color scatterer identification via Hermite function analysis, the H-scan format.

Alternatively, the ratios of the H_2/H_8 convolution outputs can be taken and used as weights for the 'R' and 'B' channels. We have chosen the lower frequency (H_2) for R and the higher frequency (H_8) for B in accordance with optical scattering.

3. Results

To demonstrate the potential of this approach to identify properties that are otherwise hidden in the conventional B-scan, a FIELD II simulation (Jensen 1996) of three scatterers are shown

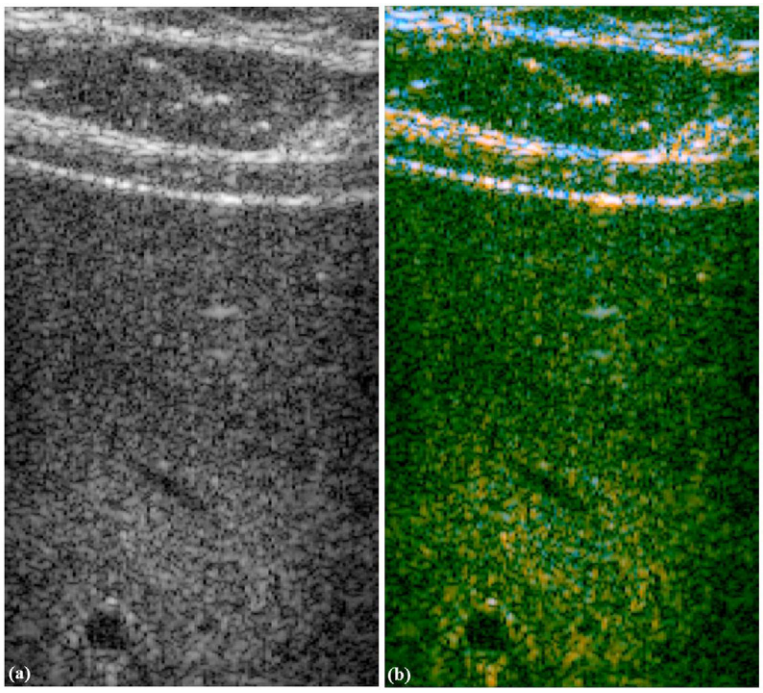

Figure 4. Five Mhz liver scan. (a) Conventional B-scan demonstrates classic speckle pattern within the liver parenchyma. (b) Hermite convolution reveals no dominant low or high frequency weighting within the liver, resulting in a green envelope as the majority signal type, with some weighting to lower frequency (orange) at maximum depths.

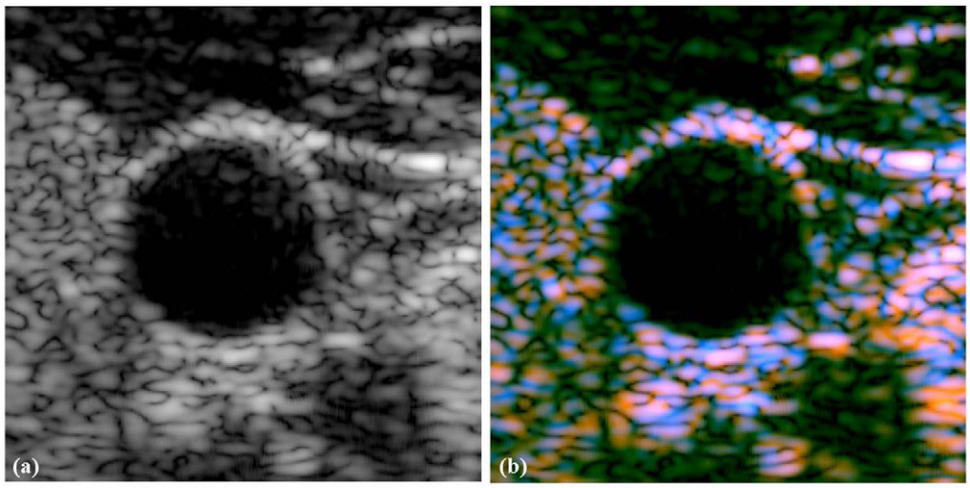

Figure 5. Five MHz transverse carotid scan, with thyroid gland to left of the carotid. (a) Conventional B-scan. (b) Hermite convolution indicates mixed blue and white patterns within the thyroid, with a smaller amount of orange.

in figure 2. Conventional imaging parameters are used including a 5 MHz center frequency linear array transducer with Gaussian apodization on transmit and receive and a 50 MHz sampling rate. However, a $\mathbf{G}H_4(t)$ round trip impulse response was implemented, scaled to a peak frequency of 5 MHz. The three scatterers were located at the transmit focus depth of 65 mm with a 7 mm lateral spacing. Importantly, the left scatterer is a conventional single impulse, the center scatterer a discrete doublet (axially), and the right scatterer a discrete triplet. Thus the scatterers approximately produce reflections that correspond to the pulse, the derivative of the pulse, and the second derivative of the pulse with respect to time. The resulting conventional B-scan image with gray scale 50 dB envelope detection is given in figure 2(a) (left) and the three scatterers appear similar with small variation in transverse width. In comparison, figure 2(b) (right, color) demonstrates the 'blue' nature of the right scatterer and the 'orange' nature of the left scatterer, consistent with their respective properties and frequency weighting according to the derivative operator and equations (2)–(4).

In the following examples, conventional B-scans are obtained using a Verasonics scanner with a 5 MHz ATL linear array transducer (Verasonics, Inc., Kirkland, WA, USA). Although conventional systems do not attempt to transmit a $\mathbf{G}H_4(t)$ function, the transmitted pulse is sufficiently similar. So an approximate analysis can be performed using the H_2 and H_8 correlation functions and then assignment of colors as described above. In the following examples, the first image shows the conventional appearance of the B-scan using standard 50 dB dynamic range on the echo envelope. The color images demonstrate convolutions with $\mathbf{G}H_2$ and $\mathbf{G}H_8$ outputs and their ratios, assigned to red and blue channels, respectively.

In order to test the analysis on random spherical scatterers, 10% gelatin phantoms were constructed with 1% by weight suspension of soft clear polyethylene microspheres (CoSpheric LLC, Santa Barbara, CA, USA). On the left side of the phantom in figures 3(a) and (b) are smaller 25 μm scatterers, (range 10–63 μm), and on the right side are larger 530 μm scatterers (range 500–600 μm). The conventional B-scan illustrates some difference in echogenicity on the left versus right sides of the phantom. In addition, the convolution with Hermite functions uncovers the key difference, as seen by the more dominant blue color on the left (small scatterers), and a more dominant orange/pink on the right (large scatterers).

A liver image from a healthy adult imaged under the requirements of informed consent and the University of Rochester Institutional Review Board is shown in figure 4. In the color identification scheme, the abdominal tissue layers are close to saturation (white), albeit with regions of orange and then blue. The liver parenchyma is largely green, indicating no strong weighting from small or large reflectors (wavelength at 5 MHz is roughly 300 μm). There is a subtle increase in orange near the deepest part of the image, possibly indicating the downshift of the propagating spectrum due to strong frequency-dependent attenuation.

Finally, a transverse carotid image is shown in figure 5. The echogenic arterial wall has both orange and blue regions within the speckle patterns. The thyroid gland, located to the left of the carotid, has a predominance of blue and white patterns, alternating with fewer but non-negligible orange regions. This may be related to the complicated glandular structure of the thyroid.

4. Discussion

Some limitations of the framework are evident. The analysis begins with simplified models of pulse echo formation and reflections. This does not capture the intricate behavior of scattering from correlated random variations in density and compressibility as were demonstrated by k-space analysis and measurements of (Campbell and Waag 1983, 1984) or by rigorous

quantitative backscatter techniques (Mottley and Miller 1988, 1990, Insana *et al* 1990, Feleppa *et al* 1997, Lizzi *et al* 1997b, Oelze *et al* 2002, Lavarello *et al* 2011, 2013). In comparison, the Hermite analysis is more simplified but has high spatial resolution. In terms of processing artifacts, two effects should be noted. As the received echo strength approaches saturation, the display reverts to white. Some additional normalization and comparison steps could be added to mitigate this nearer to the limits, but amplifier and display limits will always be present. Another effect seen in simulations is a composite of color combinations in the presence of a pure 'white noise' scattering field. Presumably due to the random spatial distribution and amplitude distribution of idealized point scatterers, some local arrangements appear as singlets, or doublets, or triplets, and other combinations. These yield different frequency responses and matching of Hermite functions. Analogous effects could exist in tissue and so interpretation of color mosaics may be complicated. Further research is required to delineate these effects and to determine the sensitivity of the approach to more subtle changes in reflection and scattering distributions.

5. Conclusion

Within a simplified framework, we have matched a convolution model of pulse reflections to the mathematics of Gaussian weighted Hermite functions. By interpreting and displaying the echoes according to their similarities to expected orders of the Hermite functions, we enable the recognition of an added dimension as each region of the echoes are characterized by their low (red), medium (green), or high (blue) frequency content as determined by the impedance function present in tissue along the direction of the propagating pulse.

Acknowledgments

The author gratefully acknowledges the expertise of PhD student Shujie Chen in programming the Verasonics scanner (Verasonics, Inc., Kirkland, WA, USA) and Mathematica notebooks (Wolfram Research, Champaign, IL, USA), greatly speeding the progress of this project. This work was supported by the Hajim School of Engineering and Applied Sciences at the University of Rochester, and was inspired by the work of Charles Hermite (1822–1901).

References

Abramowitz M and Stegun I A 1964 *United States. National Bureau of Standards. Applied Mathematics Series* (Washington, DC: US Government Publishing Office) pp 780–1

Bracewell R N 1986 *McGraw-Hill Series in Electrical Engineering. Circuits and Systems* (New York: McGraw-Hill) p 117

Burckhardt C B 1978 Speckle in ultrasound B-mode scans *IEEE Trans. Sonics Ultrason.* **25** 1–6

Campbell J A and Waag R C 1984 Ultrasonic scattering properties of three random media with implications for tissue characterization *J. Acoust. Soc. Am.* **75** 1879–86

Campbell J C and Waag R C 1983 Normalization of ultrasonic scattering measurements to obtain average differential scattering cross sections for tissues *J. Acoust. Soc. Am.* **74** 393–9

Cobbold R S C 2007 *Foundations of Biomedical Ultrasound* (New York: Oxford University Press)

Feleppa E J, Liu T, Kalisz A, Shao M C, Fleshner N, Reuter V and Fair W R 1997 Ultrasonic spectral-parameter imaging of the prostate *Int. J. Imaging Syst. Technol.* **8** 11–25

Insana M F, Wagner R F, Brown D G and Hall T J 1990 Describing small-scale structure in random media using pulse-echo ultrasound *J. Acoust. Soc. Am.* **87** 179–92

Jensen J A 1996 Field: a program for simulating ultrasound systems *10th Nordibaltic Conf. on Biomedical Imaging* pp 351–3

Lathi B P 1983 *HRW Series in Electrical and Computer Engineering* (New York: Holt Rinehart and Winston) p 500
Lavarello R J, Ghoshal G and Oelze M L 2011 On the estimation of backscatter coefficients using single-element focused transducers *J. Acoust. Soc. Am.* **129** 2903–11
Lavarello R J, Ridgway W R, Sarwate S S and Oelze M L 2013 Characterization of thyroid cancer in mouse models using high-frequency quantitative ultrasound techniques *Ultrasound Med. Biol.* **39** 2333–41
Lerner R M and Waag R C 1988 Wave space interpretation of scattered ultrasound *Ultrasound Med. Biol.* **14** 97–102
Lizzi F L, Astor M, Feleppa E J, Shao M and Kalisz A 1997a Statistical framework for ultrasonic spectral parameter imaging *Ultrasound Med. Biol.* **23** 1371–82
Lizzi F L, Astor M, Liu T, Deng C, Coleman D J and Silverman R H 1997b Ultrasonic spectrum analysis for tissue assays and therapy evaluation *Int. J Imaging Syst. Technol.* **8** 3–10
Macovski A 1983 *Medical Imaging Systems* (Englewood Cliffs, NJ: Prentice-Hall) pp 173–203
Morse P M and Ingard K U 1987 *Theoretical Acoustics* (Princeton, NJ: Princeton University Press) pp 400–66
Mottley J G and Miller J G 1988 Anisotropy of the ultrasonic backscatter of myocardial tissue: I. Theory and measurements *in vitro J. Acoust. Soc. Am.* **83** 755–61
Mottley J G and Miller J G 1990 Anisotropy of the ultrasonic attenuation in soft tissues: measurements *in vitro J. Acoust. Soc. Am.* **88** 1203–10
Oelze M L, Zachary J F and O'Brien W D Jr 2002 Characterization of tissue microstructure using ultrasonic backscatter: theory and technique for optimization using a Gaussian form factor *J. Acoust. Soc. Am.* **112** 1202–11
Poularikas A D 2010 *The Electrical Engineering Handbook Series* (Boca Raton, FL: CRC) p 7.21
Prince J L and Links J M 2006 *Ultrasound Imaging Systems* (Upper Saddle River, NJ: Pearson Prentice Hall)
Proakis J G 2001 *McGraw-Hill Series in Electrical and Computer Engineering* (Boston, MA: McGraw-Hill) pp xxi, 1002 p
Szabo T L 2004 *Diagnostic Ultrasound Imaging: Inside Out* (Burlington, MA: Elsevier Academic)
Waag R C 1984 A review of tissue characterization from ultrasonic scattering *IEEE Trans. Biomed. Eng.* **31** 884–93
Waag R C, Lee P P K, Persson H W, Schenk E A and Gramiak R 1982 Frequency-dependent angle scattering of ultrasound by liver *J. Acoust. Soc. Am.* **72** 343–52